

A second-order accurate semi-Lagrangian method for convection-diffusion equations with interfacial jumps

Hyuntae Cho, Yesom Park, and Myungjoo Kang

May 29, 2020

Abstract

In this paper, we present a second-order accurate finite-difference method for solving convection-diffusion equations with interfacial jumps on a moving interface. The proposed method is constructed under a semi-Lagrangian framework for convection-diffusion equations; a novel interpolation scheme is developed in the presence of jump conditions. Combined with a second-order ghost fluid method [3], a sharp capturing method with a first-order local truncation error near the interface and second-order truncation error away from the interface is developed for the convection-diffusion equation. In addition, a level-set advection algorithm is presented when the velocity gradient jumps across the interface. Numerical experiments support the conclusion that the proposed methods for convection-diffusion equations and level-set advection are necessary for the second-order convergence solution and the interface position.

1 Introduction

In this article, we consider the following convection-diffusion equation:

$$\begin{aligned} \rho(u_t + V \cdot \nabla u) - \nabla \cdot (\mu \nabla u) &= f \text{ in } \Omega \setminus \Gamma_t \times (0, T), \\ u &= g \text{ on } \partial\Omega \times (0, T), \\ u &= h \text{ on } \Omega \times \{0\}, \end{aligned} \tag{1.1}$$

where Ω is a bounded domain in \mathbb{R}^n ($n = 1, 2$) with boundary $\partial\Omega$ and Γ_t is a codimension-1 moving interface that divides Ω into disjoint subdomains Ω_t^+ and Ω_t^- at time $t \in (0, T)$. Furthermore, the solution for (1.1) satisfies the jump conditions

$$\begin{aligned} [\mu \frac{\partial u}{\partial \mathbf{n}}] &= b \text{ on } \Gamma_t, \\ [u] &= a \text{ on } \Gamma_t \end{aligned} \tag{1.2}$$

where \mathbf{n} is the unit normal vector to the interface Γ_t . Here, ρ and μ are positive functions that may have discontinuity across the interface, and $[q] = q^+ - q^-$ denotes the jump relation, where the superscript \pm refers to Ω^\pm . In this paper, we assume the following three conditions: (i) $[u] = a = 0$, (ii) interface Γ_t moves with velocity V , and (iii) ρ and μ are piecewise constant. Our interest in moving interface problems (1.1)–(1.2) is motivated by a desire to develop a second-order accurate method for incompressible two-phase flows [27]. The time discretization to handle incompressibility and the pressure term for the two-phase flows are important and interesting topics; however, we cannot overlook spatial discretization with jump conditions. Therefore, we consider a simplified equation (1.1) with jump conditions (1.2), which lacks the pressure term and incompressibility condition when compared with the two-phase flows. Nonetheless, it is very challenging to obtain a high-order accurate numerical method for (1.1)–(1.2) because it is sensitive to the determination of the moving interface, which is

strongly coupled to the solution and the jump condition. Thus, the aim of this study is to introduce a second-order accurate finite difference method for moving interface problems.

There are several numerical methods designed to treat jump conditions at fixed interfaces. One famous example is the immersed interface method (IIM) introduced by Leveque and Li [12]. The main idea of the IIM is to include the jump conditions in the discretization by utilizing a multivariate Taylor expansion. This was later extended in [2, 14, 15], thereby obtaining a second-order accurate solution and gradient at the interface. Recently, IIM with global second-order convergence in gradients was developed in [31]. Another is the ghost fluid method (GFM) developed by Liu et al. in [17]. The GFM introduces fictitious points to impose sharp jump conditions. While the GFM is simpler to implement than IIM, it loses accuracy due to ignorance of tangential jump conditions. To address this issue, first- and second-order extensions of GFM were developed in [6] and [3, 8] for solving elliptic interface problems. Moreover, there are other various methods for the interface problems on Cartesian grids. For examples, see the matched interface boundary method [32], virtual node method [1, 9], ghost-point multi-grid method [4], and correction function method [18, 19].

These numerical approaches have been extended to handle non-smooth solutions across the moving interface. Li [13] proposed an IIM based numerical algorithm for solving the one-dimensional nonlinear moving interface problems. Second-order convergence was obtained for the solution and interface positions, and this work has been applied to the two-phase Navier–Stokes equations when density is constant in [11, 16, 29]. Some of these methods verify second-order convergence for non-smooth solutions. However, accuracy tests with the exact solution were only conducted with stationary interface; convergence with the moving interface was not reported. On the other hand, GFM motivated various sharp capturing methods for two-phase flows [10, 25, 28, 30]. These methods succeeded in capturing jump conditions for pressure and viscous terms; however, the jump conditions were not included in the discretization of convective terms. Some methods avoid this issue by extrapolating the velocities to another region. However, second-order convergence for piecewise-smooth solutions are only reported in [25].

In this paper, we introduce a second-order accurate semi-Lagrangian method for moving interface problems (1.1)–(1.2) on a Cartesian grid. The proposed method follows the framework of the second-order ghost fluid method [3] to capture jump conditions and the level-set method [23] to track the moving interface. The main idea of this study is to incorporate jump conditions into the discretization of convection terms and diffusion terms. Our main interest is the extension of this method to the development of a second-order accurate solver of two-phase flows. Thus, we propose a solution method and an interface tracking method for nonlinear systems of moving interface problems; that is, $V = u$. The second-order convergence in both the solution and interface position is achieved.

The remainder of the paper is organized as follows: In section 2, we briefly review the level-set method and the second-order ghost fluid method. Section 3 contains the details of the numerical method for (1.1). Section 4 contains numerical experiments that validate the second-order accuracy of the proposed method.

2 Preliminaries

2.1 Level-set Method

In this study, the level-set method [23] is used to represent and capture the moving interface. The interface Γ_t is represented as a zero-level-set of a continuous function $\phi : \Omega \times [0, T] \rightarrow \mathbb{R}$:

$$\Gamma_t = \{\mathbf{x} \in \Omega \mid \phi(\mathbf{x}, t) = 0\}.$$

Furthermore, two subdomains Ω_t^+ and Ω_t^- at time t can be distinguished by the sign of the level-set function:

$$\Omega_t^+ = \{\mathbf{x} \in \Omega \mid \phi(\mathbf{x}, t) > 0\}, \quad \Omega_t^- = \{\mathbf{x} \in \Omega \mid \phi(\mathbf{x}, t) < 0\}.$$

Evolution of the interface with the velocity V is mathematically formulated as the following advection equation

$$\phi_t + V \cdot \nabla \phi = 0. \quad (2.1)$$

Another advantage of the level-set method is that the normal vector \mathbf{n} can be simply represented in terms of the level-set function:

$$\mathbf{n} = (n_x, n_y) = \left(\frac{\phi_x}{\sqrt{\phi_x^2 + \phi_y^2}}, \frac{\phi_y}{\sqrt{\phi_x^2 + \phi_y^2}} \right).$$

For more details, see [7, 22].

2.2 A second-order ghost fluid method by Cho et al. [3]

In this subsection, we briefly review the second-order ghost fluid method proposed by Cho et al. [3], focusing on the core idea of approximating u at the interface. Consider a jump condition

$$[u] = 0, [\mu \frac{\partial u}{\partial \mathbf{n}}] = b$$

on an interface Γ .

Let $\mathbf{X}_{ij} = (x_i, y_j)$ denote Cartesian grid points. Without loss of generality, assume $\mathbf{X}_{ij} \in \Omega^+$. We define local five points $\mathbf{X}_{ij}^L, \mathbf{X}_{ij}^R, \mathbf{X}_{ij}^T, \mathbf{X}_{ij}^B$, and $\mathbf{X}_{ij}^{\text{ext}}$ near \mathbf{X}_{ij} . For example, $\mathbf{X}_{ij}^R = (x_i + \theta_{ij}^R \Delta x, y_j)$ for

$$\theta_{ij}^R = \begin{cases} \frac{-D_x^0 \phi - \text{sgn}(\phi_{i,j}) \sqrt{(D_x^0 \phi)^2 - 4\phi_{i,j} D_{xx}^0 \phi}}{2D_{xx}^0 \phi} & \text{if } \phi_{i,j} \phi_{i+1,j} < 0 \\ 1 & \text{if } \phi_{i,j} \phi_{i+1,j} > 0 \end{cases}$$

where $D_x^0 \phi = \frac{\phi_{i+1,j} - \phi_{i-1,j}}{2}$ and $D_{xx}^0 \phi = \frac{\phi_{i+1,j} - 2\phi_{i,j} + \phi_{i-1,j}}{2}$. Note that $\mathbf{X}_{ij}^R = \mathbf{X}_{i+1,j}$ if $\mathbf{X}_{i+1,j} \in \Omega^+$. Conversely, if $\mathbf{X}_{i+1,j} \in \Omega^-$, \mathbf{X}_{ij}^R is the interface location on a grid segment connecting \mathbf{X}_{ij} and $\mathbf{X}_{i+1,j}$. As described in figure 2.1,

$$\mathbf{X}_{ij}^L = (x_i - \theta_{ij}^L \Delta x, y_j), \mathbf{X}_{ij}^T = (x_i, y_j + \theta_{ij}^T \Delta y), \mathbf{X}_{ij}^B = (x_i, y_j - \theta_{ij}^B \Delta y)$$

are defined in a similar manner.

Let $\mathbf{X}_{ij}^{\text{ext}}$ be any of the four points $\mathbf{X}_{i+l,j+k}$ for $l, k = -1, 1$ belonging to Ω^+ . Let $u_{ij}, u_{ij}^L, u_{ij}^R, u_{ij}^T, u_{ij}^B$ and u_{ij}^{ext} be values of u^+ at six points $\mathbf{X}_{ij}, \mathbf{X}_{ij}^L, \mathbf{X}_{ij}^R, \mathbf{X}_{ij}^T, \mathbf{X}_{ij}^B$, and $\mathbf{X}_{ij}^{\text{ext}}$, respectively. A quadratic polynomial Q is constructed to interpolate the six values of u^+ . Note that the coefficients of the quadratic polynomial Q represent a linear combination of these six values of u^+ .

For each $\mathbf{X}_{ij}^L, \mathbf{X}_{ij}^R, \mathbf{X}_{ij}^T$ and \mathbf{X}_{ij}^B , an equation is then set to approximate u at the corresponding point. First, let us consider the equation corresponding to \mathbf{X}_{ij}^R .

1. If $\mathbf{X}_{ij}^R = \mathbf{X}_{i+1,j}$, simply equate u_{ij}^R as u at grid point $\mathbf{X}_{i+1,j}$:

$$u_{ij}^R = u_{i+1,j}. \quad (2.2)$$

2. If $\mathbf{X}_{ij}^R \neq \mathbf{X}_{i+1,j}$, jump condition $[\mu u_x]$ is considered. Two different discretizations of $[\mu u_x]$ will be equated to construct the equation corresponding to \mathbf{X}_{ij}^R . First, $[\mu u_x]$ can be expressed using the jump condition of normal derivatives:

$$[\mu u_x] = [\mu u_n] n_x - [\mu] u_\tau^+ n_y, \quad (2.3)$$

where τ is the tangent vector on the interface. By discretizing u_τ^+ as $\nabla Q \cdot \tau$, one obtains a discretization of the jump condition $[\beta u_x]$. Another discretization of $[\beta u_x]$ is obtained a using

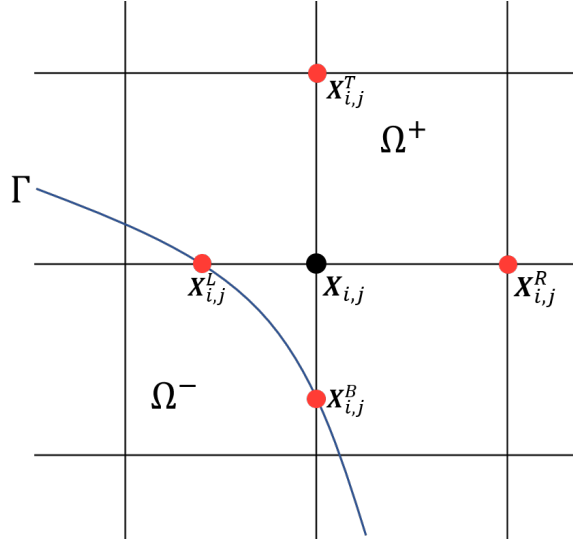


Figure 2.1: Local four points.

one-sided second-order finite difference formula. Assume that $\mathbf{X}_{i+1,j}, \mathbf{X}_{i+2,j} \in \Omega^-$, u_x^+ , and u_x^- at \mathbf{X}_{ij}^R are discretized using one-sided second-order finite difference formula:

$$\begin{aligned} u_x^+ &= \left(\frac{\theta_{ij}^R}{\theta_{ij}^L(\theta_{ij}^L + \theta_{ij}^R)} u_{ij}^L - \frac{\theta_{ij}^L + \theta_{ij}^R}{\theta_{ij}^L \theta_{ij}^R} u_{i,j} + \frac{2\theta_{ij}^R + \theta_{ij}^L}{\theta_{ij}^R(\theta_{ij}^L + \theta_{ij}^R)} u_{ij}^R \right) / \Delta x, \\ u_x^- &= \left(-\frac{3 - 2\theta_{ij}^R}{(1 - \theta_{ij}^R)(2 - \theta_{ij}^R)} u_{ij}^R + \frac{2 - \theta_{ij}^R}{1 - \theta_{ij}^R} u_{i+1,j} - \frac{1 - \theta_{ij}^R}{2 - \theta_{ij}^R} u_{i+2,j} \right) / \Delta x. \end{aligned} \quad (2.4)$$

Two discretizations are combined to construct the equation corresponding to \mathbf{X}_{ij}^R :

$$[\beta u_n] n_x - [\beta] (\nabla Q \cdot \tau) n_y = \beta^+ u_x^+ - \beta^- u_x^-. \quad (2.5)$$

In addition, an equation similar to either (2.2) or (2.5) is obtained for each $\mathbf{X}_{ij}^L, \mathbf{X}_{ij}^T$ and \mathbf{X}_{ij}^B . Combining these four equations, we derive the following linear system

$$\mathbf{M} \begin{pmatrix} u_{ij}^R \\ u_{ij}^L \\ u_{ij}^T \\ u_{ij}^B \end{pmatrix} = \mathbf{N} \mathbf{u} + \mathbf{D}, \quad (2.6)$$

where $\mathbf{M}, \mathbf{N}, \mathbf{D}$ are real-valued vectors or matrices of appropriate size, and \mathbf{u} is a vector consisting of values of u at the grid points. By solving system (2.6), we get expressions of $u_{ij}^L, u_{ij}^R, u_{ij}^T, u_{ij}^B$ as linear combinations of u at the grid points plus the constants.

Remark Note that it cannot be guaranteed that $\mathbf{X}_{i+2,j} \in \Omega^-$ when discretizing (2.4). Assuming each domain Ω^+ and Ω^- is connected, one simple approach to handle such a case is to set $\mathbf{X}_{ij}^R = \mathbf{X}_{i+2,j}$, $\theta_R = 2$ and $u_{ij}^R = u_{i+2,j}$. For a detailed explanation of discretizing jump conditions when $\mathbf{X}_{i+2,j} \in \Omega^+$, see [3].

3 Numerical methods

A collocated grid is used, so all values of ϕ and u are located at Cartesian grid points \mathbf{X}_{ij} , even when u is vector-valued. To implicitly discretize the diffusive term in (1.1), the normal vector \mathbf{n} and the interface position at the next time level is needed. Thus, ϕ^{n+1} is updated before u^{n+1} . Once the level-set is advected, u is solved using the semi-Lagrangian method combined with the backward difference formula. A concise outline of the overall algorithm is given as follows:

1. Evolve the level-set function and reinitialize it. (Before evolution of the level-set function, extrapolate u^n at the interface to the grid points when $\mathbf{V} = u$)
2. Trace back departure points and apply the interpolation procedure to discretize convective term via semi-Lagrangian method.
3. Construct a linear system corresponding to backward difference discretization and solve it for u .

In the following sections, each step is explained in detail.

3.1 Evolution of level-set

The level-set function is updated from ϕ^n to ϕ^{n+1} with the velocity field V . To give the consistency with the overall methodology, we use the second-order semi-Lagrangian method

$$\frac{3\phi_{ij}^{n+1} - 4\phi_d^n + \phi_d^{n-1}}{2\Delta t} = 0 \quad (3.1)$$

to discretize (2.1). The departure points are traced backward by a second-order Runge-Kutta method. The quadratic ENO interpolation procedure is then applied to recover the values of ϕ at the departure points. For more details, see [21].

The evolution (2.1) often leads numerical distortion of the level-set function near the interface. To avoid this problem, ϕ^{n+1} is reinitialized to the signed distance function, by solving the following pseudo-time dependent Eikonal equation:

$$\phi_\xi + \text{sgn}(\phi^0) (\|\nabla\phi\| - 1) = 0.$$

Here, sgn denotes the signum function whose value is either -1, 0, or 1. For reinitialization, a Gauss-Seidel temporal discretization, in conjunction with ENO finite differences [20], is used.

3.1.1 Velocity extrapolation off the interface

In cases where $V = u$, the interface moves with velocity u . However, the discontinuity in gradient of u causes first-order accuracy for the level-set function ϕ , even with second-order semi-Lagrangian method and second-order reinitialization. Therefore, ϕ should be evolved with an alternative velocity field W that has continuous gradients and agrees with u on the interface, i.e. $W|_\Gamma = u|_\Gamma$. To construct such W , we adopt the extension algorithm technique with sub-cell resolution used in [5, 6]. The method extends u to be a constant along the curve normal for Γ . This suggests the following pseudo-time dependent partial differential equation:

$$\begin{aligned} \frac{\partial W}{\partial \xi} + \text{sign}(\phi)\mathbf{n} \cdot \nabla W &= 0, \\ W &= u \text{ on } \Gamma, \end{aligned} \quad (3.2)$$

whose characteristics are normal for Γ .

Assuming $\phi_{ij} > 0$, the equation is semi-discretized as

$$\frac{W_{ij}^{l+1} - W_{ij}^l}{\Delta \xi_{ij}} + (n_x^+ D_x^- W_{ij} + n_x^- D_x^+ W_{ij} + n_y^+ D_y^- W_{ij} + n_y^- D_y^+ W_{ij}) = 0,$$

where $n_x^+ = \max(n_x, 0)$ and $n_x^- = \min(n_x, 0)$. Second-order ENO scheme with sub-cell resolution technique is used for spatial discretization.

$$D_x^- W_{ij} = \begin{cases} \frac{W_{ij} - W_{i-1,j}}{\Delta x} + \frac{\min\text{mod}(D_{xx}^0 W_{ij}, D_{xx}^0 W_{i-1,j})}{2\Delta x} & \text{if } \phi_{ij} \phi_{i-1,j} > 0 \\ \frac{W_{ij} - u_{ij}^L}{\theta_{ij}^L \Delta x} + \theta_{ij}^L \frac{\min\text{mod}(D_{xx}^0 W_{ij}, D_{xx}^0 W_{i-1,j})}{2\Delta x} & \text{if } \phi_{ij} \phi_{i-1,j} \leq 0 \end{cases},$$

$$D_x^+ W_{ij} = \begin{cases} \frac{W_{i+1,j} - W_{i,j}}{\Delta x} - \frac{\min\text{mod}(D_{xx}^0 W_{ij}, D_{xx}^0 W_{i+1,j})}{2\Delta x} & \text{if } \phi_{ij} \phi_{i+1,j} > 0 \\ \frac{u_{ij}^R - W_{ij}}{\theta_{ij}^R \Delta x} - \theta_{ij}^R \frac{\min\text{mod}(D_{xx}^0 W_{ij}, D_{xx}^0 W_{i+1,j})}{2\Delta x} & \text{if } \phi_{ij} \phi_{i+1,j} \leq 0 \end{cases}.$$

$D_y^- W_{ij}$ and $D_y^+ W_{ij}$ are similarly defined. We take a grid dependent time step $\Delta \xi_{ij}$ in order to avoid small time steps imposed at the grid points close to the interface. In particular, we set

$$\Delta \xi_{ij} = \min(\theta_{ij}^R, \theta_{ij}^L, \theta_{ij}^T, \theta_{ij}^B) \times CFL \Delta x$$

And use the second-order Runge-Kutta formula for temporal discretization. In actual implementation, we take $CFL = 0.4$ and the algorithm is performed up to 20 iterations. After W is obtained, the level-set function is advected with the extrapolated velocity W .

3.2 Semi-Lagrangian ghost fluid method(SL-GFM)

Quadratic and bilinear interpolation only attain first-order accuracy near the interface due to the discontinuity of gradients. Thus, we introduce a new interpolation scheme in conjunction with the ghost fluid method which provides second-order accuracy near the interface. Exploiting the jump conditions in computing the values of u at the departure points is the main idea for improving performance near the interface. We name the semi-Lagrangian method with the proposed interpolation procedure the semi-Lagrangian ghost fluid method (SL-GFM).

3.2.1 Backward Integration

We track the departure points by the second-order Runge-Kutta

$$\hat{\mathbf{X}} = \mathbf{X}_{ij} - \frac{\Delta t}{2} V^n(\mathbf{X}_{ij})$$

$$\mathbf{X}_d^n = \mathbf{X}_{ij} - \Delta t V^{n+\frac{1}{2}}(\hat{\mathbf{X}}).$$

The velocity at the half time step $t^{n+\frac{1}{2}}$ is approximated by the second-order extrapolation

$$V^{n+\frac{1}{2}} = \frac{3}{2} V^n - \frac{1}{2} V^{n-1}.$$

Similarly, the departure point at the time step $n-1$ is estimated by

$$\hat{\mathbf{X}} = \mathbf{X}_{ij}^{n+1} - \Delta t V^n(\mathbf{X}_{ij})$$

$$\mathbf{X}_d^{n-1} = \mathbf{X}_{ij}^{n+1} - 2\Delta t V^n(\hat{\mathbf{X}}).$$

We impose a restriction on the time step size as

$$\Delta t < \frac{\Delta x}{2 \|V\|_\infty}$$

to ensure the departure points locate in an adjacent cell. That is,

$$|x_d - x_i| < \Delta x$$

$$|y_d - y_j| < \Delta y.$$

3.2.2 Interpolation procedures

Let us focus on the interpolation procedure of the semi-Lagrangian method. Let u_d^n denote the approximation of u at the point \mathbf{X}_d^n . Without loss of generality, assume $\mathbf{X}_d^n \in [x_i, x_{i+1}] \times [y_j, y_{j+1}]$. Although $\mathbf{X}_{ij} \in \Omega_{t^{n+1}}^+$ does not guarantee that $\mathbf{X}_d^n \in \Omega_{t^n}^+$ and $\mathbf{X}_d^{n-1} \in \Omega_{t^{n-1}}^+$ due to numerical error, we assume $\phi(\mathbf{X}_d^n, t^n) > 0$ if $\phi_{ij}^{n+1} > 0$ and $\phi(\mathbf{X}_d^n, t^n) < 0$ if $\phi_{ij}^{n+1} < 0$ during the interpolation procedure. For simplicity, in this section we omit subscripts and superscripts corresponding to time. The most natural choice for approximating u_d is the bilinear interpolation

$$u_d = u_{ij}(1 - \theta_x)(1 - \theta_y) + u_{i+1,j}\theta_x(1 - \theta_y) + u_{i,j+1}(1 - \theta_x)\theta_y + u_{i+1,j+1}\theta_x\theta_y, \quad (3.3)$$

where $\theta_x = \frac{x_d - x_i}{\Delta x}$, $\theta_y = \frac{y_d - y_j}{\Delta y} \in (0, 1)$.

We can construct a quadratic interpolation by correcting (3.3) with second-order derivatives. Let us define a discrete operator

$$D_{xx}^0 u_{ij} = u_{i+1,j} - 2u_{ij} + u_{i-1,j}. \quad (3.4)$$

For numerical stability of the interpolation, u_{xx}^0 is set to be one of $D_{xx}^0 u_{ij}$, $D_{xx}^0 u_{i+1,j}$, $D_{xx}^0 u_{i,j+1}$, and $D_{xx}^0 u_{i+1,j+1}$, which has the minimum absolute value; u_{yy}^0 is defined in duplication. These values lead to quadratic ENO interpolation

$$\begin{aligned} u_d = & u_{ij}(1 - \theta_x)(1 - \theta_y) + u_{i+1,j}\theta_x(1 - \theta_y) \\ & + u_{i,j+1}(1 - \theta_x)\theta_y + u_{i+1,j+1}\theta_x\theta_y - u_{xx}^0 \frac{\theta_x(1 - \theta_x)}{2} - u_{yy}^0 \frac{\theta_y(1 - \theta_y)}{2}. \end{aligned} \quad (3.5)$$

The interpolation (3.5) is third-order accurate for smooth u . However, one cannot guarantee that all grid points involved in the interpolation belong to same subdomain with \mathbf{X}_d . To address this issue, we introduce the following notions. We say the point \mathbf{X}_d is *regular* if all grid points involved in the quadratic ENO interpolation belong to the same region with \mathbf{X}_d . Otherwise, \mathbf{X}_d is called *irregular*. In SL-GFM, the quadratic ENO interpolation is used for regular \mathbf{X}_d and the modified bilinear interpolation is used for irregular \mathbf{X}_d . The modified bilinear interpolation is constructed by replacing the interpolating value to the ghost value as follows.

Suppose \mathbf{X}_d is irregular and there exists at least one grid point out of \mathbf{X}_{ij} , $\mathbf{X}_{i+1,j}$, $\mathbf{X}_{i,j+1}$, $\mathbf{X}_{i+1,j+1}$ that belongs to the same region with \mathbf{X}_d . Without loss of generality, we may assume $\mathbf{X}_d \in \Omega^+$ and $\mathbf{X}_{ij} \in \Omega^-$. Next, using u_{ij} with the bilinear interpolation (3.3) would produce $O(\Delta x)$ error. Alternatively, we replace this with u_{ij}^+ , which is the extended value of u^+ at \mathbf{X}_{ij} obtained by using the second-order GFM.

If $\mathbf{X}_{i+1,j} \in \Omega^+$, the point \mathbf{X}_{ij}^R is located on the interface. One possible ghost value of u_{ij}^+ can be computed by an extrapolation from u_{ij}^R and $u_{i+1,j}$:

$$\frac{\theta_{ij}^R}{1 - \theta_{ij}^R} (u_{ij}^R - u_{i+1,j}) + u_{ij}^R.$$

Similarly, if $\mathbf{X}_{i,j+1} \in \Omega^+$, u_{ij}^+ can be approximated as

$$\frac{\theta_{ij}^T}{1 - \theta_{ij}^T} (u_{ij}^T - u_{i,j+1}) + u_{ij}^T.$$

When the extrapolations from the both directions are available, as shown in figure 3.1a, the direction with the smaller distance is chosen. When both $\mathbf{X}_{i+1,j}$, $\mathbf{X}_{i,j+1} \in \Omega^-$, as shown in figure 3.1b, u_{ij}^+ is approximated from $u_{i+1,j+1}$:

$$u_{i+1,j+1} + \frac{1}{1 - \theta_{i,j+1}^R} (u_{i,j+1}^R - u_{i+1,j+1}) + \frac{1}{1 - \theta_{i+1,j}^T} (u_{i+1,j}^T - u_{i+1,j+1}).$$

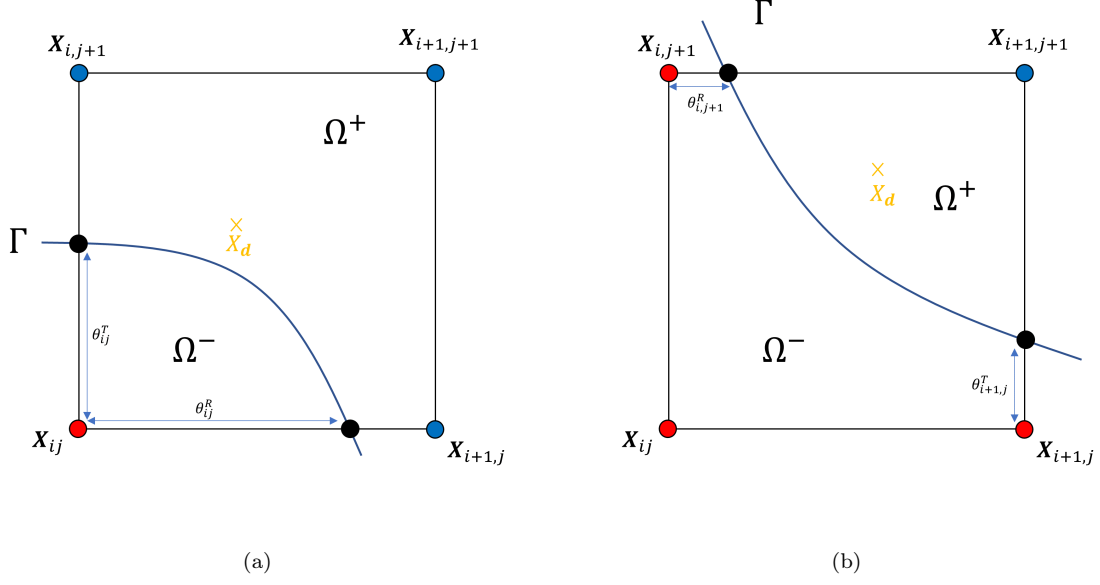


Figure 3.1: Grid points near the interface

In summary we derive the following formula:

$$u_{ij}^+ = \begin{cases} u_{ij} & \text{if } \mathbf{X}_{ij} \in \Omega^+ \\ \frac{1}{1-\theta_{ij}^R} u_{ij}^R - \frac{\theta_{ij}^R}{1-\theta_{ij}^R} u_{i+1,j} & \text{else if } \mathbf{X}_{i+1,j} \in \Omega^+ \text{ and } \theta_{ij}^R \leq \theta_{ij}^T \\ \frac{1}{1-\theta_{ij}^T} u_{ij}^T - \frac{\theta_{ij}^T}{1-\theta_{ij}^T} u_{i,j+1} & \text{else if } \mathbf{X}_{i,j+1} \in \Omega^+ \text{ and } \theta_{ij}^T \leq \theta_{ij}^R \\ \frac{\theta_{i,j+1}^R \theta_{i+1,j}^T - 1}{(1-\theta_{i,j+1}^R)(1-\theta_{i+1,j}^T)} u_{i+1,j+1} + \frac{1}{1-\theta_{i,j+1}^R} u_{i,j+1}^R + \frac{1}{1-\theta_{i+1,j}^T} u_{i+1,j}^T & \text{otherwise.} \end{cases}$$

A similar process is used to define the ghost values $u_{i+1,j}^+$, $u_{i,j+1}^+$ and $u_{i+1,j+1}^+$, which correspond to points $\mathbf{X}_{i+1,j}$, $\mathbf{X}_{i,j+1}$, and $\mathbf{X}_{i+1,j+1}$, respectively. Following this, we adopt the bilinear interpolation to approximate u_d at Ω^+ :

$$u_d = u_{ij}^+ (1 - \theta_x) (1 - \theta_y) + u_{i+1,j}^+ \theta_x (1 - \theta_y) + u_{i,j+1}^+ (1 - \theta_x) \theta_y + u_{i+1,j+1}^+ \theta_x \theta_y. \quad (3.6)$$

Due to numerical errors, it is not guaranteed that at least one of \mathbf{X}_{ij} , $\mathbf{X}_{i+1,j}$, $\mathbf{X}_{i,j+1}$, or $\mathbf{X}_{i+1,j+1}$ belongs to Ω^+ . In other words, the ghost values of u^+ may not be defined, so the interpolation from Ω^+ is not possible on the cell. In such a case, u_d is approximated via the bilinear interpolation on the four points in Ω^- . To justify the approximation, we briefly prove the following statement:

$$u^+(\mathbf{X}_d) = u_d + O(\Delta x^2).$$

Let

$$\phi_d = \phi_{ij} (1 - \theta_x) (1 - \theta_y) + \phi_{i+1,j} \theta_x (1 - \theta_y) + \phi_{i,j+1} (1 - \theta_x) \theta_y + \phi_{i+1,j+1} \theta_x \theta_y.$$

Since the bilinear interpolation is second-order accurate, we have

$$|\phi_d - \phi(\mathbf{X}_d)| = O(\Delta x^2). \quad (3.7)$$

In addition, the condition $\mathbf{X}_{ij}, \mathbf{X}_{i+1,j}, \mathbf{X}_{i,j+1}, \mathbf{X}_{i+1,j+1} \in \Omega^-$ leads to

$$\phi_d < 0. \quad (3.8)$$

From (3.7), (3.8) together with $\mathbf{X}_d \in \Omega^+$, we obtain

$$\phi(\mathbf{X}_d) = O(\Delta x^2).$$

Since ϕ is a signed distance function, there exist $\mathbf{X}_\Gamma \in \Gamma$, such that $|\mathbf{X}_d - \mathbf{X}_\Gamma| = O(\Delta x^2)$. Thus, we may conclude that

$$\begin{aligned} |u_d - u^+(\mathbf{X}_d)| &\leq |u_d - u^-(\mathbf{X}_d)| + |u^-(\mathbf{X}_d) - u^-(\mathbf{X}_\Gamma)| + |u^+(\mathbf{X}_\Gamma) - u^+(\mathbf{X}_d)| \\ &\leq O(\Delta x^2) + O(\Delta x^2) + O(\Delta x^2) = O(\Delta x^2). \end{aligned}$$

Here, we used the facts that $|u(\mathbf{X}_\Gamma) - u(\mathbf{X}_d)| \leq |\nabla u|_\infty |\mathbf{X}_\Gamma - \mathbf{X}_d| + O(\Delta x^2) = O(\Delta x^2)$ and $u^-(\mathbf{X}_\Gamma) = u^+(\mathbf{X}_\Gamma)$.

3.3 Linear system

When \mathbf{X}_d^n and \mathbf{X}_d^{n-1} are both regular with respect to time t^n and t^{n-1} , a second-order backward differentiation formula(BDF) is adopted. Namely,

$$\rho \frac{3u_{ij}^{n+1} - 4u_d^n + u_d^{n-1}}{2\Delta t} = \mu \Delta_h u_{ij}^{n+1} + f_{ij}^{n+1}.$$

On the other hand, if one of \mathbf{X}_d^n and \mathbf{X}_d^{n-1} is irregular, first-order BDF is used for time discretization:

$$\rho \frac{u_{ij}^{n+1} - u_d^n}{\Delta t} = \mu \Delta_h u_{ij}^{n+1} + f_{ij}^{n+1}.$$

Following the second-order GFM, the standard finite difference method of the five-point Laplacian formula is used to discretize the elliptic operator at the grid points away from the interface $\Gamma_{t^{n+1}}$:

$$\Delta_h u_{ij}^{n+1} = \frac{u_{i+1,j}^{n+1} - 2u_{ij}^{n+1} + u_{i-1,j}^{n+1}}{\Delta x^2} + \frac{u_{i,j+1}^{n+1} - 2u_{ij}^{n+1} + u_{i,j-1}^{n+1}}{\Delta y^2}.$$

If grid segments for each Cartesian direction intersect with the interface, the Laplacian formula is discretized using the Shortley-Weller method [26]

$$\begin{aligned} \Delta_h u_{ij}^{n+1} &= \left(\frac{u_{ij}^R - u_{ij}^{n+1}}{\theta_{ij}^R \Delta x} - \frac{u_{ij}^{n+1} - u_{ij}^L}{\theta_{ij}^L \Delta x} \right) \Bigg/ \left(\frac{\theta_{ij}^R + \theta_{ij}^L}{2} \Delta x \right) \\ &\quad + \left(\frac{u_{ij}^T - u_{ij}^{n+1}}{\theta_{ij}^T \Delta x} - \frac{u_{ij}^{n+1} - u_{ij}^B}{\theta_{ij}^B \Delta y} \right) \Bigg/ \left(\frac{\theta_{ij}^T + \theta_{ij}^B}{2} \Delta y \right), \end{aligned}$$

where $u_{ij}^R, u_{ij}^L, u_{ij}^T$ and u_{ij}^B are computed according to section 2.2. μ and ρ are defined naturally, as

$$\rho = \begin{cases} \rho^+ & \text{if } \mathbf{X}_{ij} \in \Omega_{t^{n+1}}^+ \\ \rho^- & \text{if } \mathbf{X}_{ij} \in \Omega_{t^{n+1}}^- \end{cases}, \quad \mu = \begin{cases} \mu^+ & \text{if } \mathbf{X}_{ij} \in \Omega_{t^{n+1}}^+ \\ \mu^- & \text{if } \mathbf{X}_{ij} \in \Omega_{t^{n+1}}^- \end{cases}.$$

Combining all, we attain a linear system whose coefficient matrix is non-symmetric. Since $u_{ij}^R, u_{ij}^L, u_{ij}^T$ and u_{ij}^B are used in the interpolation at the next time step, we save these in actual implementation.

Remark The numerical method proposed throughout previous sections allows us to solve parabolic moving interface problems

$$\rho u_t - \nabla \cdot (\mu \nabla u) = f.$$

Except for the semi-Lagrangian application owing to the absence of advection terms, the second-order BDF

$$\rho \frac{3u_{ij}^{n+1} - 4u_{ij}^n + u_{ij}^{n-1}}{2\Delta t} = \nabla \cdot (\beta \nabla u_i^{n+1}) + f_i^{n+1}$$

can be used to design a second-order accurate scheme. If $\phi_{ij}^{n+1} > 0$ but $\phi_{ij}^n < 0$, implicit time discretization with ghost value u_{ij}^+ , which was introduced in 3.2.2, is used:

$$\rho \frac{u_{ij}^{n+1} - u_{ij}^+}{\Delta t} = \nabla \cdot (\beta \nabla u_i^{n+1}) + f_i^{n+1}.$$

4 Numerical results

In this section, several numerical experiments are carried out to verify second-order accuracy in the L^∞ norm of the proposed method. Throughout this section, the linear system in section 3.3 is solved by the generalized minimal residual method (GMRES) with an incomplete LU preconditioner [24]. All numerical experiments are carried out in C++ on a personal computer. Unless the source term f or the jump condition $[\mu \frac{\partial u}{\partial \mathbf{n}}]$ is specifically mentioned, it is computed according to the exact solution u and ϕ .

4.1 Scalar equation : Translation

We begin with an accuracy test in a simple setting. Consider a translating circular interface Γ_t with velocity $V = (1, 1)$ on a computational domain $\Omega = [-2, 2]^2$. Specifically, the interface Γ_t is defined as the zero level-set of a function

$$\phi(x, y, t) = \sqrt{(x - t + 0.5)^2 + (y - t + 0.5)^2} - 1.$$

With the parameters

$$\rho^- = 1, \quad \rho^+ = 1, \quad \mu^- = 1, \quad \mu^+ = 2$$

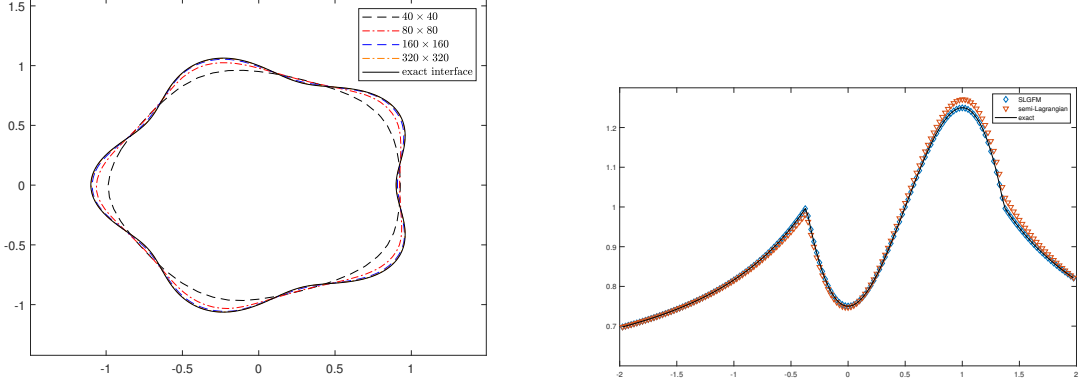
and the source term

$$f(x, y, t) = \begin{cases} 4\mu^-(2x - 2t + 1); & \text{in } \Omega^- \\ \frac{\mu^+(2y - 2t + 1)}{2((x - t + 0.5)^2 + (y - t + 0.5)^2)^{\frac{3}{2}}} & \text{in } \Omega^+ \end{cases},$$

the exact solution is given by

$$u(x, y, t) = \begin{cases} -(x - t + 0.5) \left((x - t + 0.5)^2 + (y - t + 0.5)^2 - 1 \right) & \text{in } \Omega^- \\ \frac{y - t + 0.5}{\sqrt{(x - t + 0.5)^2 + (y - t + 0.5)^2}} - (y - t + 0.5) & \text{in } \Omega^+ \end{cases}.$$

We compare the results obtained by our method and SL-BDF2, which uses the conventional quadratic ENO interpolation with the semi-Lagrangian method. Table 1 shows the convergence results with the time step $\Delta t = 0.4\Delta x$ and at the final time $T = 1$. Figure 4.1 shows the corresponding solutions on the 160×160 grid. Though the SL-BDF2 also discretizes diffusive terms using a ghost-fluid method [3], overall accuracy is first-order. Besides, we can see that the SL-GFM yields second-order convergence. The difference between these two results is the applied interpolation scheme; hence, it indicates the necessity of using the proposed interpolation method. It can also be confirmed from figure 4.1 that the SL-GFM approximates the solution u much more accurately than the SL-BDF2.



(a) Graph of u by SL-GFM

(b) Cross section of u at $y = 1$ by SL-GFM(diamond) and SL-BDF2(triangle) with the exact value(solid line)

Figure 4.1: Solution of test 1 on a 160×160 grid.

Grid	SL-BDF2		SL-GFM	
	$\ u(x, y, t) - u_{ij}\ _\infty$	order	$\ u(x, y, t) - u_{ij}\ _\infty$	order
40^2	1.34×10^{-1}	-	1.05×10^{-2}	-
80^2	6.70×10^{-2}	1.00	2.62×10^{-3}	2.00
160^2	3.29×10^{-2}	1.03	7.02×10^{-4}	1.90
320^2	1.65×10^{-2}	1.00	1.82×10^{-4}	1.95
640^2	8.27×10^{-3}	0.99	4.60×10^{-5}	1.98

Table 1: Convergence rates for test 1.

4.2 Scalar equation : Rotation

As a second example, a flower shaped interface rotating around the origin with a unit angular velocity $V = (-y, x)$ in a domain $\Omega = [-2, 2]^2$ is chosen. The interface can be described by the level function in polar coordinates

$$\phi(x, y, t) = r - 1 - 0.1 \cos(5(\theta - t)).$$

Parameters are chosen to $\rho^- = 100, \rho^+ = 1, \mu^- = 10$ and $\mu^+ = 1$ with the exact solution

$$u(x, y, t) = \begin{cases} r^2 - 1 & \text{in } \Omega^- \\ 0.1 \cos(5(\theta - t)) (2 + 0.1 \cos(5(\theta - t))) & \text{in } \Omega^+. \end{cases}$$

Since $\|V\|_\infty = 4$ on Ω , we set the time step restriction as $\Delta t = 0.2\Delta x$. Results at the final time $T = \pi$, when the interface Γ_t completes half a rotation, are presented in table 2. These results show that SL-GFM offers better accuracy when compared with SL-BDF2. The accuracy at low resolutions tends to be lower than second-order; however, this is due to the slow convergence of the interface position and the normal vector, which is evaluated from the level-set function. Referring to figure 4.2, convergence of the interface position is followed by the second-order convergence of the solution on finer resolution.

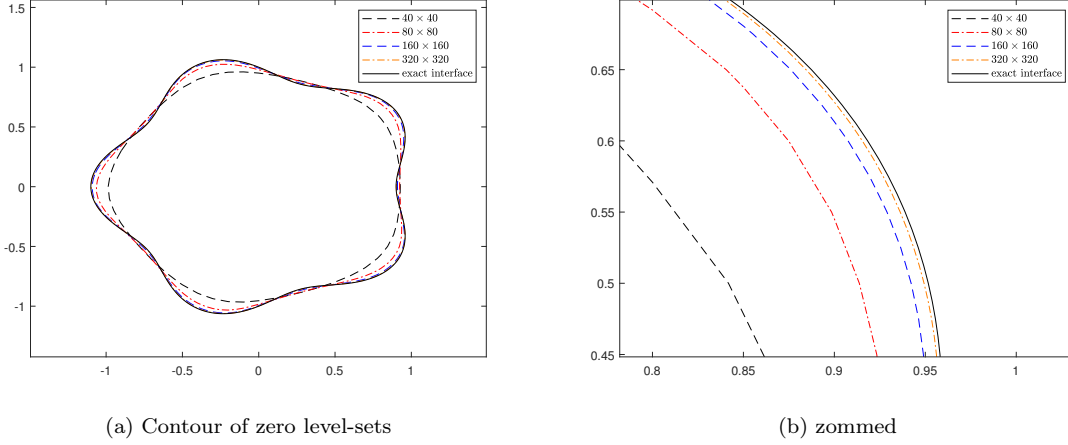


Figure 4.2: Interface position of example 2 at $t = \pi$ on various grids.

Grid	SL-BDF2		SL-GFM	
	$\ u(x, y, t) - u_{ij}\ _\infty$	order	$\ u(x, y, t) - u_{ij}\ _\infty$	order
40^2	2.17×10^{-1}	-	1.62×10^{-1}	-
80^2	1.34×10^{-1}	0.69	7.48×10^{-2}	1.11
160^2	6.61×10^{-2}	1.02	2.15×10^{-2}	1.80
320^2	2.95×10^{-2}	1.16	6.01×10^{-3}	1.84
640^2	1.42×10^{-2}	1.06	1.57×10^{-3}	1.94

Table 2: Convergence rates for test 2.

4.3 Scalar equation : Deformation

Consider a deforming interface

$$\Gamma_t = \{(x, y) \in \mathbb{R}^2 | x^2 \left(1 - \frac{3}{4}t\right) + y^2 \left(1 - \frac{1}{2}t\right) = 1\}. \quad (4.1)$$

It is easy to see that Γ_t is a unit circle at $t = 0$ and moves with the velocity

$$V(x, y, t) = \left[\frac{3x}{8 - 6t}, \frac{y}{4 - 2t} \right],$$

to become an ellipse. Two methods are tested with solution

$$u(x, y, t) = \begin{cases} \left(1 - \frac{5}{8}t\right) (x^2 + y^2) + 4t & \text{in } \Omega^- \\ \frac{1}{8}t (x^2 - y^2) + 4t & \text{in } \Omega^+ \end{cases}.$$

and quantities $\rho^- = 1, \rho^+ = 100, \mu^- = 1, \mu^+ = 10$. In this simulation, we used the time step restriction $\Delta t = 0.1\Delta x$. The accuracy at the final time $T = 1$ is presented in table 3. Figure 4.3 depicts the numerical solution obtained by the SL-GFM carried out on a 160×160 grid. It shows that the SL-GFM leads to second-order convergence, but the SL-BDF2 only results in the first-order accuracy.

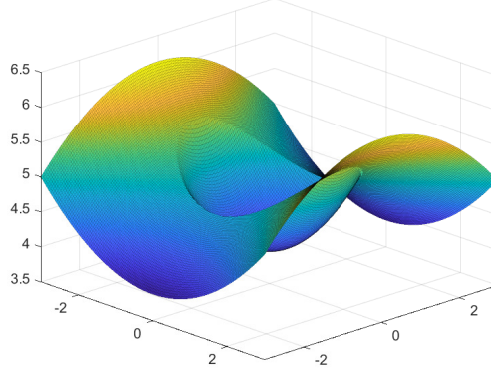


Figure 4.3: Solution of test 3 on 160×160 grid.

Grid	SL-BDF2		SL-GFM	
	$\ u(x, y, t) - u_{ij}\ _\infty$	order	$\ u(x, y, t) - u_{ij}\ _\infty$	order
40^2	1.01×10^{-1}	-	2.72×10^{-2}	-
80^2	7.77×10^{-2}	0.38	7.93×10^{-3}	1.78
160^2	4.59×10^{-2}	0.76	2.18×10^{-3}	1.86
320^2	2.60×10^{-2}	0.82	5.84×10^{-4}	1.90
640^2	1.43×10^{-2}	0.86	1.48×10^{-4}	1.97

Table 3: Convergence rates for test 3.

4.4 Non-linear system : Translation

We now consider a non-linear system, which occurs when $V = u$. On a computational domain $\Omega = [-2, 2]^2$, the interface is given as the zero level-set of a function

$$\phi(x, y, t) = \sqrt{(x - t + 0.5)^2 + (y - t + 0.5)^2} - 1,$$

and the solution $u = (u^1, u^2)$ is given as

$$u^1(x, y, t) = \begin{cases} 1 & \text{in } \Omega^- \\ 1 + \frac{1}{2} \log((x - t + 0.5)^2 + (y - t + 0.5)^2) & \text{in } \Omega^+ \end{cases}$$

and

$$u^2(x, y, t) = \begin{cases} 1 & \text{in } \Omega^- \\ 1 - \frac{1}{2} \log((x - t + 0.5)^2 + (y - t + 0.5)^2) & \text{in } \Omega^+ \end{cases}.$$

It is easy to see that $u|_\Gamma = (1, 1)$, which agrees with the velocity of the interface. Jump conditions are

$$\left[\mu \frac{\partial u}{\partial \mathbf{n}} \right] = (\mu^+, \mu^-).$$

Three different numerical experiments, using different methods for level-set advection, are conducted with $\rho^+ = 1, \rho^- = 1000$ and $\mu^+ = 0.1, \mu^- = 10$ up to $t = 1$. See figure 4.4 for the profile of the solution.

First, let u_{ij}^a, ϕ_{ij}^a denote numerical solutions of u and ϕ when the level-set function is advected with the velocity u^n at each step. Next, let u_{ij}^b, ϕ_{ij}^b be numerical solutions when the extrapolation technique discussed in section 3.1.1 is used to determine the velocity at which the level-set moves. Finally, u_{ij}^c denotes a numerical solution of u when ϕ is given exactly. Numerical errors for these solutions are presented in table 4. In addition, L^∞ errors of ϕ are computed only at the grid points, such that $|\phi| < 3 \max(\Delta x, \Delta y)$. Despite the same method being applied to u in these three tests, we can observe a huge difference between them due to the accuracy of tracking the interface. When ϕ is advected with u but without the extrapolation technique, both u_{ij}^a and ϕ_{ij}^a show first-order accuracy. However, when ϕ is computed with the extrapolated velocity, second-order convergence is obtained for both u_{ij}^b and ϕ_{ij}^b . Furthermore, when the interface is given exactly, we see that u_{ij}^c shows the lowest error among all three experiments. Since the jump conditions $[\mu \frac{\partial u}{\partial \mathbf{n}}]$ are dependent on normal vectors, a second-order accurate interface position and normal vector are needed to obtain a second-order accurate solution u .

Table 4: Convergence rates for example 4

(a) solution

Grid	$\ u(x, y, t) - u_{ij}^a\ _\infty$	order	$\ u(x, y, t) - u_{ij}^b\ _\infty$	order	$\ u(x, y, t) - u_{ij}^c\ _\infty$	order
40^2	2.30×10^{-2}	-	1.24×10^{-2}	-	1.76×10^{-3}	-
80^2	9.52×10^{-3}	1.27	3.19×10^{-3}	1.95	4.87×10^{-4}	1.85
160^2	4.57×10^{-3}	1.06	9.13×10^{-4}	1.81	1.28×10^{-4}	1.92
320^2	2.19×10^{-3}	1.06	2.53×10^{-4}	1.85	3.29×10^{-5}	1.97
640^2	1.10×10^{-3}	1.00	6.33×10^{-5}	2.00	8.31×10^{-6}	1.98

(b) interface

Grid	$\ \phi(x, y, t) - \phi_{ij}^a\ _\infty$	order	$\ \phi(x, y, t) - \phi_{ij}^b\ _\infty$	order
40^2	2.37×10^{-2}	-	1.36×10^{-2}	-
80^2	9.90×10^{-3}	1.26	3.33×10^{-3}	2.03
160^2	4.88×10^{-3}	1.02	9.38×10^{-4}	1.83
320^2	2.27×10^{-3}	1.11	2.56×10^{-4}	1.87
640^2	1.14×10^{-3}	1.00	6.39×10^{-5}	2.00

4.5 Non-linear system : Rotation

Consider a circular interface Γ_t that rotates around the origin, which is given as a zero level-set of a function

$$\phi(x, y, t) = \sqrt{(x - 1.5 \cos(t))^2 + (y - 1.5 \sin(t))^2} - 1$$

on computational domain $[-3, 3]^2$. Hence, we conducted the accuracy test for the following solution

$$u^1(x, y, t) = \begin{cases} -y & \text{in } \Omega^- \\ -y + \frac{1}{2} \log((x - 1.5 \cos(t))^2 + (y - 1.5 \sin(t))^2) & \text{in } \Omega^+ \end{cases}.$$

and

$$u^2(x, y, t) = \begin{cases} x & \text{in } \Omega^- \\ x + \frac{1}{2} \log((x - \cos(t))^2 + (y - \sin(t))^2) & \text{in } \Omega^+ \end{cases}.$$

f and $[\mu \frac{\partial u}{\partial \mathbf{n}}]$ are given according to the solution. Numerical simulations are performed up to $t = \pi$ with quantities $\rho^+ = 1000, \rho^- = 1, \mu^+ = 10, \mu^- = 0.1$. Second-order convergences in L^∞ norm of the solution and the interface position for both cases are presented in table 5.

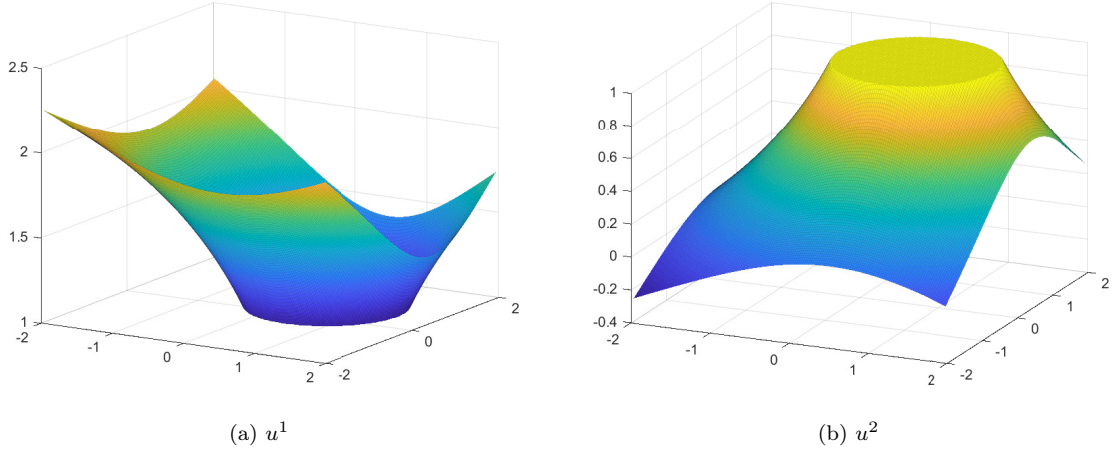


Figure 4.4: Solution of test 4 on 160×160 grid.

Table 5: Convergence rates for example 5

Grid	$\ u(x, y, t) - u_{ij}\ _\infty$	order	$\ \phi(x, y, t) - \phi_{ij}\ _\infty$	order
40^2	4.56×10^{-1}	-	4.05×10^{-1}	-
80^2	9.64×10^{-2}	2.24	1.10×10^{-1}	1.88
160^2	2.80×10^{-2}	1.78	3.03×10^{-2}	1.86
320^2	6.65×10^{-3}	2.08	7.05×10^{-3}	2.11
640^2	1.79×10^{-3}	1.90	1.28×10^{-3}	2.47

4.6 Non-linear equation in 3D: Translation

We now consider the example in 3D. Interface Γ_t is a moving sphere, which is represented as a zero level-set of function

$$\phi(x, y, z, t) = \sqrt{(x + 0.5 - t)^2 + (y + 0.5 - t)^2 + (z + 0.5 - t)^2} - 1.$$

For the exact solution

$$u(x, y, z, t) = \begin{cases} 1 & \text{in } \Omega^- \\ \frac{1}{\sqrt{(x+0.5-t)^2+(y+0.5-t)^2+(z+0.5-t)^2}} & \text{in } \Omega^+ \end{cases},$$

the velocity field is set as $V = (u, u, u)$. Since $u|_{\Gamma_t} = 1$, movement of the interface Γ_t agrees with V . Numerical simulations are conducted up to final time $T = 1$ with quantities $\rho^+ = 1, \rho^- = 100$, and $\mu^+ = 1, \mu^- = 10$. Convergence results and average iteration number of GMRES for each time step, denoted as N_g , are presented in table 6. A second-order convergence of SL-GFM in 3D is verified; the iteration number does not dramatically increase.

Table 6: Convergence rates for example 6

Grid	$\ u(x, y, z, t) - u_{ijk}\ _\infty$	order	$\ \phi(x, y, z, t) - \phi_{ijk}\ _\infty$	order	N_g
40^3	1.37×10^{-2}	-	1.47×10^{-2}	-	16
80^3	3.63×10^{-3}	1.92	3.70×10^{-3}	1.99	23
160^3	9.63×10^{-4}	1.91	9.60×10^{-4}	1.95	32

5 Conclusion

In this paper, a second-order accurate finite difference method for solving convection diffusion equations with jump conditions on a moving interface is presented. A bilinear interpolation using the ghost values near the interface is developed and adopted to the interpolation procedure of the semi-Lagrangian method. Coupled with second-order ghost fluid method [3], this produces a second-order convergence in L^∞ norms. Furthermore, we have presented a second-order algorithm for an evolving interface when the velocity has jumps in its normal derivatives. Under the assumption that second-order time-discretization of two-phase incompressible flow is provided, we expect that the proposed method can be used to develop a second-order sharp capturing method for incompressible two-phase flows.

References

- [1] Bedrossian, J., Von Brecht, J.H., Zhu, S., Sifakis, E., Teran, J.M.: A second order virtual node method for elliptic problems with interfaces and irregular domains. *Journal of Computational Physics* **229**(18), 6405–6426 (2010)
- [2] Chen, X., Feng, X., Li, Z.: A direct method for accurate solution and gradient computations for elliptic interface problems. *Numerical Algorithms* **80**(3), 709–740 (2019)
- [3] Cho, H., Han, H., Lee, B., Ha, Y., Kang, M.: A second-order boundary condition capturing method for solving the elliptic interface problems on irregular domains. *Journal of Scientific Computing* **81**(1), 217–251 (2019)
- [4] Coco, A., Russo, G.: Second order finite-difference ghost-point multigrid methods for elliptic problems with discontinuous coefficients on an arbitrary interface. *Journal of Computational Physics* **361**, 299–330 (2018)
- [5] Dalmon, A., Kentheswaran, K., Mialhe, G., Lalanne, B., Tanguy, S.: Fluids-membrane interaction with a full eulerian approach based on the level set method. *Journal of Computational Physics* **406**, 109171 (2020)
- [6] Egan, R., Gibou, F.: xgfm: Recovering convergence of fluxes in the ghost fluid method. *Journal of Computational Physics* p. 109351 (2020)
- [7] Gibou, F., Fedkiw, R., Osher, S.: A review of level-set methods and some recent applications. *Journal of Computational Physics* **353**, 82–109 (2018)
- [8] Guittet, A., Lepilliez, M., Tanguy, S., Gibou, F.: Solving elliptic problems with discontinuities on irregular domains—the voronoi interface method. *Journal of Computational Physics* **298**, 747–765 (2015)
- [9] Hellrung Jr, J.L., Wang, L., Sifakis, E., Teran, J.M.: A second order virtual node method for elliptic problems with interfaces and irregular domains in three dimensions. *Journal of Computational Physics* **231**(4), 2015–2048 (2012)
- [10] Kang, M., Fedkiw, R.P., Liu, X.D.: A boundary condition capturing method for multiphase incompressible flow. *Journal of Scientific Computing* **15**(3), 323–360 (2000)
- [11] Lee, L., LeVeque, R.J.: An immersed interface method for incompressible navier–stokes equations. *SIAM Journal on Scientific Computing* **25**(3), 832–856 (2003)
- [12] Leveque, R.J., Li, Z.: The immersed interface method for elliptic equations with discontinuous coefficients and singular sources. *SIAM Journal on Numerical Analysis* **31**(4), 1019–1044 (1994)

- [13] Li, Z.: Immersed interface methods for moving interface problems. *Numerical Algorithms* **14**(4), 269–293 (1997)
- [14] Li, Z.: A fast iterative algorithm for elliptic interface problems. *SIAM Journal on Numerical Analysis* **35**(1), 230–254 (1998)
- [15] Li, Z., Ji, H., Chen, X.: Accurate solution and gradient computation for elliptic interface problems with variable coefficients. *SIAM journal on numerical analysis* **55**(2), 570–597 (2017)
- [16] Li, Z., Lai, M.C.: The immersed interface method for the navier–stokes equations with singular forces. *Journal of Computational Physics* **171**(2), 822–842 (2001)
- [17] Liu, X.D., Fedkiw, R.P., Kang, M.: A boundary condition capturing method for poisson’s equation on irregular domains. *Journal of computational Physics* **160**(1), 151–178 (2000)
- [18] Marques, A.N., Nave, J.C., Rosales, R.R.: A correction function method for poisson problems with interface jump conditions. *Journal of Computational Physics* **230**(20), 7567–7597 (2011)
- [19] Marques, A.N., Nave, J.C., Rosales, R.R.: High order solution of poisson problems with piecewise constant coefficients and interface jumps. *Journal of Computational Physics* **335**, 497–515 (2017)
- [20] Min, C.: On reinitializing level set functions. *Journal of computational physics* **229**(8), 2764–2772 (2010)
- [21] Min, C., Gibou, F.: A second order accurate level set method on non-graded adaptive cartesian grids. *Journal of Computational Physics* **225**(1), 300–321 (2007)
- [22] Osher, S., Fedkiw, R., Piechor, K.: Level set methods and dynamic implicit surfaces. *Appl. Mech. Rev.* **57**(3), B15–B15 (2004)
- [23] Osher, S., Sethian, J.A.: Fronts propagating with curvature-dependent speed: algorithms based on hamilton-jacobi formulations. *Journal of computational physics* **79**(1), 12–49 (1988)
- [24] Saad, Y.: *Iterative methods for sparse linear systems*, vol. 82. siam (2003)
- [25] Schroeder, C., Stomakhin, A., Howes, R., Teran, J.M.: A second order virtual node algorithm for navier–stokes flow problems with interfacial forces and discontinuous material properties. *Journal of Computational Physics* **265**, 221–245 (2014)
- [26] Shortley, G.H., Weller, R.: The numerical solution of laplace’s equation. *Journal of Applied Physics* **9**(5), 334–348 (1938)
- [27] Sussman, M., Smereka, P., Osher, S., et al.: A level set approach for computing solutions to incompressible two-phase flow (1994)
- [28] Sussman, M., Smith, K.M., Hussaini, M.Y., Ohta, M., Zhi-Wei, R.: A sharp interface method for incompressible two-phase flows. *Journal of computational physics* **221**(2), 469–505 (2007)
- [29] Tan, Z., Le, D.V., Li, Z., Lim, K.M., Khoo, B.C.: An immersed interface method for solving incompressible viscous flows with piecewise constant viscosity across a moving elastic membrane. *Journal of Computational Physics* **227**(23), 9955–9983 (2008)
- [30] Theillard, M., Gibou, F., Saintillan, D.: Sharp numerical simulation of incompressible two-phase flows. *Journal of Computational Physics* **391**, 91–118 (2019)
- [31] Tong, F., Wang, W., Feng, X., Zhao, J., Li, Z.: How to obtain an accurate gradient for interface problems? *Journal of Computational Physics* **405**, 109070 (2020)
- [32] Zhou, Y., Zhao, S., Feig, M., Wei, G.W.: High order matched interface and boundary method for elliptic equations with discontinuous coefficients and singular sources. *Journal of Computational Physics* **213**(1), 1–30 (2006)